Original Article
PRKD3 promotes proliferation of liver cancer cells: a downstream proteomics profiling study

Ye Tian[1,2*], Bei Xie[2*], Shuaiyang Wang[1], Xingyuan Ma[1], Haohua Deng[1], Lei Ma[1], Linjing Li[1]

[1]Department of Clinical Laboratory Center, Lanzhou University Second Hospital, Lanzhou 730030, Gansu, China; [2]Department of Immunology, School of Basic Medical Sciences, Lanzhou University, Lanzhou 730030, Gansu, China. *Equal contributors.

Abstract: Background: Protein kinase D 3 (PRKD3), a serine/threonine protein kinase, functions as a crucial regulator across numerous cancer types. However, its regulatory function and mechanism in hepatocellular carcinoma (HCC) proliferation remain unclear. *In vitro* experiments and proteomics analysis offer new insights into the regulation and mechanism of PRKD3 in HCC. Methods: A PRKD3 knockdown cell line was constructed to assess the effects of PRKD3 on proliferation of HCC cells using cell counting kit-8 (CCK-8) assay, 5-Ethynyl-2'-deoxyuridine (EdU) assay, clonogenic assay, and flow cytometry. Proteomic changes in liver cancer cells before and after PRKD3 knockdown were analyzed using 4D-lablefree technology. Results: Analysis of The Cancer Genome Atlas (TCGA) dataset revealed abnormal PRKD3 expression in HCC, associated with poorer prognosis and specific pathological types. Results from the CCK-8 assay showed a marked reduction in the proliferation of Huh7 cells ($P < 0.01$), with the number of clonal colonies being 5.26 times higher than that in PRKD3 knockdown cells, and the EdU positivity rate decreased from 54.77% to 37.97%. Flow cytometry results indicated that PRKD3 knockout induced cell cycle arrest at G2/M phase. Proteomic analysis revealed 330 proteins had altered expression, associated with amino acid transport, stress response, and apoptosis. Cyclin-dependent kinase 4 (CDK4), plasminogen activator inhibitor 1 (SERPINE1), sequestosome 1 (SQSTM1), ras-related protein Rab-8A (RAB8A), and nuclear receptor-binding factor 2 (NRBF2) emerged as key nodes in the protein interaction network. Conclusion: This study elucidates the inhibitory effect of PRKD3 knockdown on HCC proliferation and unveils the proteomic features of PRKD3 regulation. CDK4, SERPINE1, SQSTM1, RAB8A, and NRBF2 may serve as key proteins in PRKD3's regulatory pathways.

Keywords: PRKD3, liver cancer, Huh7, proliferation, proteomic

Introduction

According to data from the World Health Organization (https://www.iarc.who.int/), the number of liver cancer patients has reached 860,000, ranking sixth among all cancer types, with a death toll of 750,000, placing it third among all cancers. However, the incidence and mortality rates of liver cancer are notably higher in Asia, especially in China and Southeast Asia, compared to the global average.

Protein kinase D (PRKD), a serine/threonine kinase, includes three closely related members: PRKD1, PRKD2, and PRKD3. Studies have demonstrated that PRKD3 is variably expressed across different cancers and cancer cell lines, functioning as an oncoprotein. It reg-ulates the expression and signal transduction of multiple key tumor genes through various pathways, affecting the malignant phenotype of tumors [1-8]. PRKD3 was reported to promote cell proliferation by activating mTORC1-S6K1 in triple-negative breast cancer cells [1]. Further observations indicate that PRKD3 facilitates proliferation and survival of prostate cancer cells by modulating AKT serine/threonine kinase 1 activity [9, 10].

High mRNA and protein levels of PRKD3 were reported to be associated with multiple tumor nodules, vascular infiltration, advanced AJCC staging, and poor prognosis in patients with hepatocellular carcinoma (HCC) after liver resection [11], highlighting the oncogenic function of PRKD3. However, the specific functions

of PRKD3 at the cellular level in liver cancer cells, as well as the differential protein expression affected by PRKD3 remain to be explored. There is little research on the regulatory mechanism and downstream network of PRKD3 in HCC. Investigating PRKD3 at the cellular level can help clarify the specific functions of PRKD3, guiding future in vivo studies and clinical trials. This research can provide a new theoretical basis for the diagnosis and treatment of liver cancer.

The aim of this study was to investigate the role of PRKD3 by analyzing cell proliferation and cell cycle in a stable PRKD3 knockdown cell model. Additionally, 4D-label-free technology and bioinformatics analysis were employed to investigate the downstream protein networks regulated by PRKD3, providing a new theoretical basis for understanding the role of PRKD3 in promoting carcinogenesis in HCC and identifying key downstream pathways.

Methods

Collection of data

The TCGA database, a publicly funded project, provides gene expression data and sequencing data for various cancers, along with patient-specific clinical data. RNA-sequencing expression profiles and corresponding clinical information for different tumors, including liver hepatocellular carcinoma (LIHC), were retrieved from this dataset. Kaplan-Meier curve, p value, and hazard ratio (HR) with a 95% confidence interval (CI) were generated using log-rank tests and univariate Cox proportional hazards regression.

Cell culture and transfection

Human liver cancer Huh7 cells were maintained in our laboratory and cultured in a 5% CO_2 environment at 37°C using Dulbecco modified Eagle medium (DMEM) supplemented with 10% fetal bovine serum (FBS). The PRKD3 cell knockdown model was established by transfecting cells with PRKD3 short hairpin RNA (shRNA) using lentivirus. Huh7 cells were inoculated onto a 6-well plate with 1×10^5 cells per well. After 24 hours, the appropriate amount of virus, based on MOI=20 and its titer, was added. Cells were incubated at 37°C for 16 hours, and the culture medium was replaced

with fresh complete medium, and cells were cultured for an additional 56 hours. The transfection efficiency was determined by observing the fluorescence intensity of the cells. The PRKD3 knockdown group was designated as shPRKD3, while the control group cells were set as shNC. The shRNA targeting sequence for PRKD3: CCGGGCCAGTTTGGCATCGTTTATGCTC-GAGCATAAACGATGCCAAACTGGCTTTTTG, AATT-CAAAAAGCCAGTTTGGCATCGTTTATGCTCGA-GCATAAACGATGCCAAACTGGC. The knockdown efficiency of PRKD3 was verified through Western blot (WB) and quantitative real-time PCR (qRT-PCR).

Western blot

Cells were lysed with RIPA buffer and centrifuged at 12,000 rpm for 10 min. Protein lysates were separated by SDS-PAGE, transferred to a PVDF membrane, and incubated overnight at 4°C with antibodies against rabbit anti-PRKD3 (1:1000, CST), anti-CDK4 (1:1000, ImmunoWay), anti-SERPINE1 (1:1000, CST), anti-SQSTM1 (1:1000, Abcam), anti-RAB8A (1:1000, CST), anti-NRBF2 (1:1000, CST), and anti-GAPDH (1:1000, Servicebio), all diluted at 1:1000. The membranes were then incubated with a secondary antibody, goat anti-rabbit IgG (1:5000, ImmunoWay), and visualized using enhanced chemiluminescence.

qRT-PCR

Total RNA was extracted from harvested cells using Trizol reagent and reverse transcribed into cDNA following the manufacturer's protocols. Quantitative RT-PCR amplification and detection were performed using a Quant Studio 3 system (ABI, American) with SYBR Green dye (Yeason, China) and 10 μM forward and reverse primers. The specific primer sequences used for qRT-PCR included PRKD3 forward primer: CTGCTTCTCCGTGTTCAAGTC; PRKD3 reverse primer: GAGGCCAATTTGCAGTAGAAATG; GAPDH forward primer: TGACTTCAACAGCGACACCCA; GAPDH reverse primer: CACCCTGTTGCTGTAG-CCAAA.

Cell counting kit-8 (CCK-8)

Lentivirus-infected cells from different groups were seeded into 96-well plates at a density of 8,000 cells per well. Cell viability was assessed using CCK-8 assays at 1, 2, 3, 4, and 5 days

after seeding by adding 10 µL of CCK-8 solution (Biosharp, China) to each well and incubating for 1.5 hours at 37°C. The absorbance at 450 nm was measured to determine cell viability.

Colony formation assay

For the colony formation assay, 4,000 cells were seeded in 6-well plates. Lentivirus-infected Huh7 cells were cultured for approximately seven days, washed with PBS, fixed with 4% paraformaldehyde for two minutes, and stained with 0.1% crystal violet solution. After washing with distilled water, pictures were taken, and the number of colonies was counted using Image J V1.53 software.

Ethynyl Deoxyuridine (EdU) proliferation assay

The EdU proliferation assay (Beyotime Biotechnology, China) was conducted to measure cell proliferation. Cells were seeded in 6-well plates (1×10^5 cells/well) with 1 mL of 10% serum-containing DMEM for 24 hours. Cells were then incubated with 10 µM EdU in DMEM for 2.5 hours. After fixation, washing, and adding the click additive solution for 30 minutes, nuclei were stained with Hoechst 33342 (Beyotime, China) for 15 minutes. Cell proliferation was observed under a fluorescence microscope (Nikon eclipse Ti2-E, Japan).

Cell apoptosis assay

Cell apoptosis was detected using Annexin V-APC/7-AAD double staining method. Approximately 1×10^6 cells were digested with EDTA-free trypsin, resuspended, and centrifuged at 1000 rpm for 5 minutes. Cells were subsequently resuspended in 500 µL of binding buffer and incubated with 5 µL of Annexin V-APC (BD, USA) and 10 µL of 7-AAD for 5 minutes in a dark environment to facilitate staining. After setting the Forward Scatter (FSC), side scatter (SSC), and fluorescence channel voltage and compensation, analysis was performed using flow cytometry (NovoCyte Quanteon, Agilent, USA).

Cell cycle assay

For the cell cycle assay, 1×10^5 lentivirus-infected Huh7 cells were seeded into each well of 6-well plates and incubated in a CO_2 environment at 37°C 24 hours. Subsequently, cells were washed twice with PBS, harvested, col-

lected, and fixed overnight at -20°C using 70% cooled ethanol. For staining, the cells were incubated in a PI solution for 30 minutes. Analysis was conducted using flow cytometry (NovoCyte Quanteon, Agilent, USA), with NovoExpress-V1.5.6 software employed to evaluate the distribution of cells across different phases of the cell cycle.

Collection and preparation of proteomic samples

After culture, 5×10^6 cells were collected and lysed using SDT lysis buffer and rapidly frozen in liquid nitrogen to preserve the protein samples. Subsequently, protein concentration was measured utilizing BCA assay, and 50 µg of the protein sample was prepared for enzymatic hydrolysis using the filter-aided sample preparation (FASP) method.

LC-MS/MS

The mass spectrometry signals of the sample were acquired using the 4D-lable free method with a High-Performance Liquid Chromatography NanoElute system (Bruker, Germany). Buffer A consisted of a 0.1% formic acid aqueous solution and buffer B of a 0.1% formic acid in acetonitrile. The chromatographic columns were equilibrated with 95% Buffer A, and samples were loaded from the automatic sampler onto the loading column (Thermo Scientific Acclaim PepMap100, Thermo Fisher Scientific, USA), which was then separated by an analytical column (Thermo Scientific EASY analytical column, Thermo Fisher Scientific, USA). The gradient elution process was as follows: 0-50 minutes, Buffer B increased from 0 to 35%; 50-55 minutes, it ramped from 35 to 100%; 55-60 minutes, it was held at 100%. The autosampler temperature was set at 4°C, and the chromatographic column was at ambient temperature. The separated samples were analyzed using a timsTOF Pro mass spectrometer (Bruker, Germany) with an electrospray voltage of 1.5 kV. The mass spectrometry scanning range was set to 100-1700 m/z, using Parallel Accumulation Serial Fragmentation (PASEF) mode for data collection.

Data analysis

Data obtained were analyzed using MaxQuant-V1.6.14 software. The settings parameters

included trypsin digestion with up to two missing cleavages allowed; Peptide mass tolerance was set at 6 ppm and fragment mass tolerance at 20 ppm; fixed modification was Carbamidomethyl (C), and variable modification was Oxidation (M). Results were filtered with a Q value cutoff of 0.01 (corresponding to 1% FDR), and proteins were identified based on at least two unique peptides. Protein quantification was calculated by summing the intensities of razor and unique peptides.

Identification and cluster analysis of differential proteins

Differential expression of proteins between groups was determined using fold change and *p* value (T-test) as criteria. Proteins with fold change > 2 or < 0.5 and *P* < 0.05 were considered significantly downregulated and upregulated, respectively.

Gene Ontology (GO) functional enrichment analysis

Proteins were categorized by GO annotation into three groups: biological process (BP), cellular compartment (CC), and molecular function (MF). Two-tailed Fisher's exact test was used to examine the enrichment of differentially expressed proteins against all identified proteins within each category, considering a corrected *P* < 0.05 as significant.

Kyoto Encyclopedia of Genes and Genomes (KEGG) functional enrichment analysis

The KEGG Automatic Annotation Server (KAAS) was used to annotate the KEGG pathways of differentially expressed proteins. The distribution of differentially expressed proteins in the KEGG pathway was analyzed. Significant enrichment *p* value was calculated using hypergeometric distribution tests, and the FDR was corrected using Benjamin - Hochberg multiple tests to determine KEGG functional enrichment of differentially expressed proteins.

Protein-protein interaction network

Analysis of different proteins in STRING database yielded direct or indirect interaction between proteins. The connectivity of the top 25 core proteins was recalculated, and a network diagram and protein expression histogram were created.

Results

Higher PRKD3 was correlated with malignancy and poor survival in LIHC

The expression of PRKD3 in several malignant tumour tissues in the TCGA dataset revealed that LIHC was one of the tumours with substantial PRKD3 expression (**Figure 1A**, **1B**). Further analysis of LIHC clinical information from the dataset showed that PRKD3 expression levels were associated with LIHC histology and increased with advancing grades (**Figure 1C**, **1D**). Kaplan-Meier survival analyses indicated that high PRKD3 expression was associated with significantly shorter survival in LIHC patients (**Figure 1E**).

Establishment of a PRKD3 knockdown cell model

We initially selected six types of liver cancer cells and detected the basal expression level of PRKD3. It showed that PRKD3 was highly expressed in all six types of liver cancer cells. Considering the cultivation and *in vivo* experimental plans in the future, we chose Huh7 cells for subsequent knockdown model construction.

To explore oncoprotein function of PRKD3 in HCC tumorigenesis, the effective transfection by lentivirus and the subsequent downregulation of PRKD3 in Huh7 cells were confirmed, with most cells expressing green fluorescent protein, indicating a successful transfection (**Figure 2A**). The expression of PRKD3 mRNA in transfected cells and control cells was detected by qRT-PCR. Compared with the shNC, the shPRKD3 group showed a significant decrease (56.8%) in PRKD3 mRNA expression (*P* < 0.01) (**Figure 2B**). WB showed that the expression of PRKD3 protein in the shPRKD3 group was lower than that in the shNC group (**Figure 2C**), which was consistent with the mRNA expression results.

Interference of PRKD3 suppressed the proliferation ability of HCC cells

The impact of PRKD3 on Huh7 cell growth was further examined using CCK-8, colony formation, and EdU assays. The CCK-8 assay revealed a significant decrease in absorbance at 450 nm in the shPRKD3 group of cells compared to the shNC group (*P* < 0.01) (**Figure 3A**). Colony
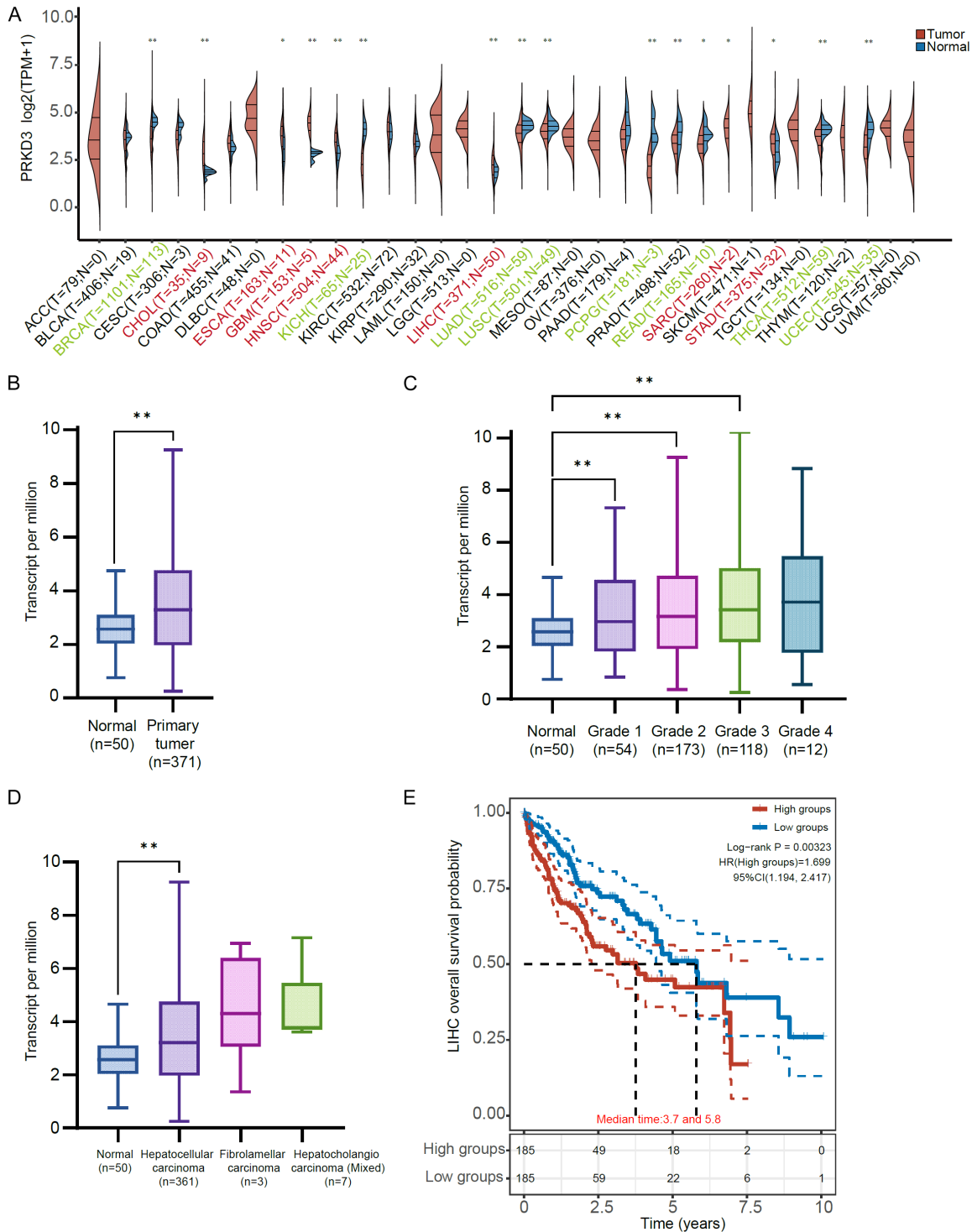
Figure 1. Expression of Protein kinase D 3 (PRKD3) and clinical characteristics of liver hepatocellular carcinoma (LIHC). (A) The expression distribution of PRKD3 in tumor and normal tissues; (B-D) PRKD3 expression classified by sample types (B), tumor grade (C) and tumor histology (D); (E) Prognostic value of PRKD3 expression in LIHC. Results are displayed as the mean ± SD. *$P < 0.05$; **$P < 0.01$.

formation assay showed that the shNC group formed significantly more cell clusters (828.00 ± 78.08) than the shPRKD3 group (157.33 ±

29.37), a 5.26-fold difference ($P < 0.01$) (**Figure 3B**). The EdU assay indicated a decrease in proliferation rate from (54.77 ± 8.692)% in the
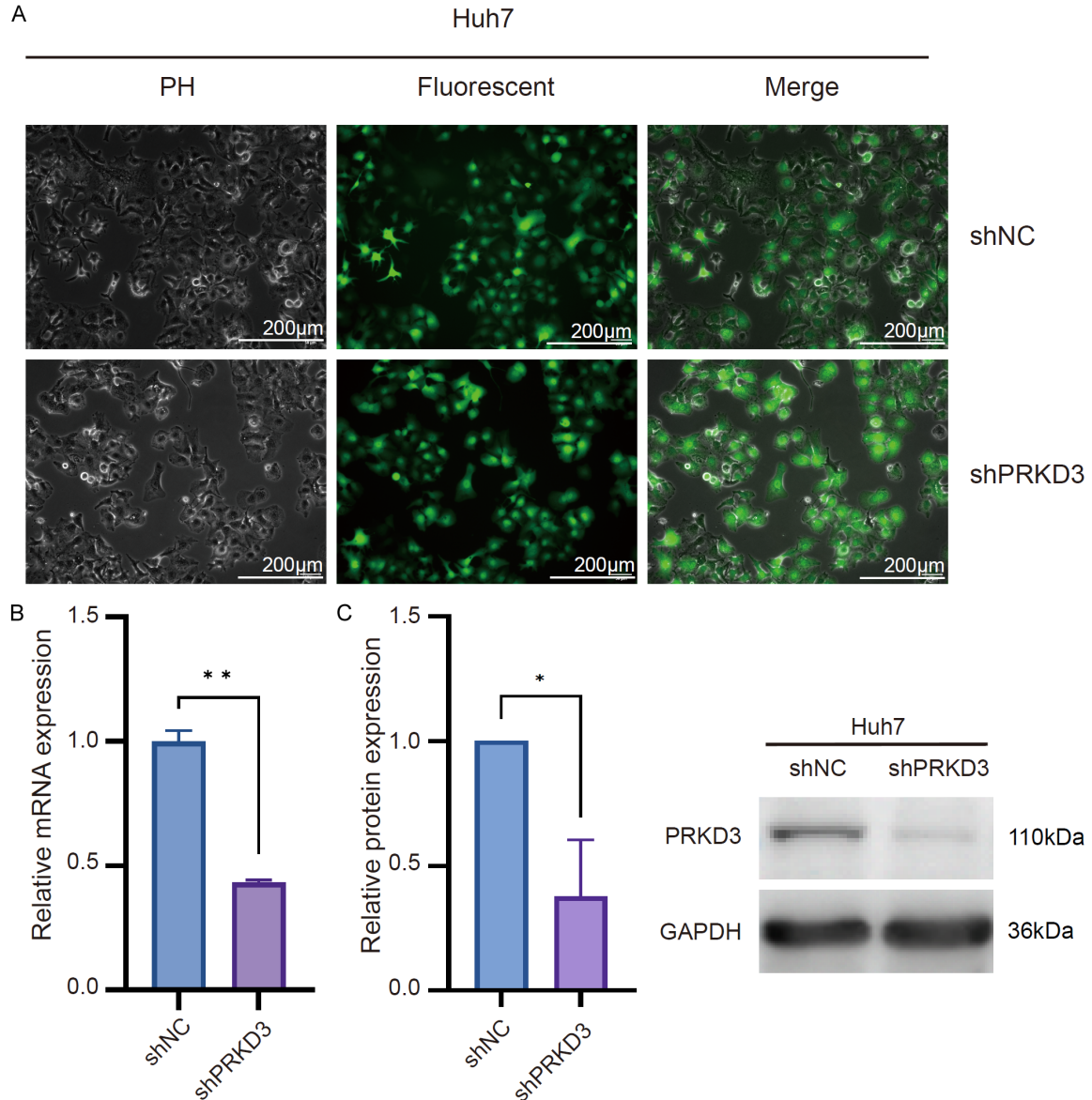
Figure 2. Construction of Protein kinase D 3 (PRKD3) knockdown Huh7 cell lines. A. Green fluorescence indicates the transfection of lentivirus; B. PRKD3 mRNA expression levels in Huh7 cells infected with different lentivirus detected by Quantitative real-time PCR (qRT-PCR); C. PRKD3 protein expression levels Huh7 cells transfected with different lentivirus detected by Western blot (WB). Results are displayed as the mean ± SD. *$P < 0.05$; **$P < 0.01$, n=3.

shNC group to (37.97 ± 3.96)% in the shPRKD3 group ($P < 0.01$) (**Figure 3C**). These results collectively suggest that PRKD3 knockdown inhibits the proliferation of Huh7 liver cancer cells.

Knockdown of PRKD3 induced apoptosis and cell cycle arrest in HCC cells

Apoptosis of Huh7 cells was assessed using annexin V-APC and 7-AAD staining, with flow cytometry revealing a significant increase in the apoptosis rate following PRKD3 knockdown. The shNC group had an apoptosis rate of 0.08%, while the shPRKD3 group exhibited an average apoptosis rate of 19.71% (**Figure 4A**). Additionally, PRKD3 silencing resulted in an increased proportion of cells in the G2/M phase and a reduced proportion in the S phase, indicating cell cycle arrest in the G2/M phase in HCC cells (**Figure 4B**). Thus, PRKD3 knockdown suppresses HCC cell growth through the induction of S-G2/M cell cycle arrest.
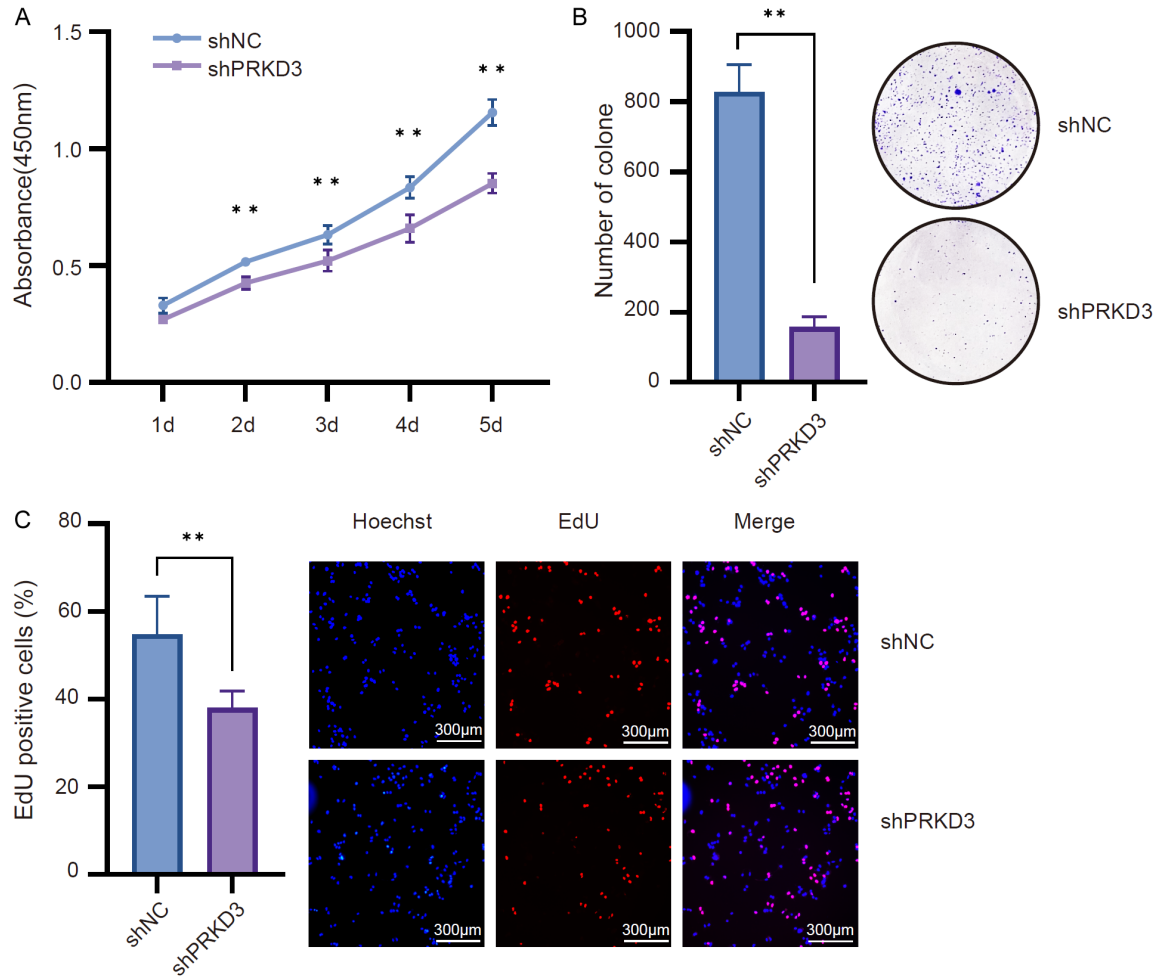
Figure 3. Knockdown of Protein kinase D 3 (PRKD3) suppressed Huh7 cells growth. A. At 1 d, 2 d, 3 d, 4 d and 5 d after transfection, cell counting kit-8 (CCK-8) detected that PRKD3 knockdown reduced the Huh7 cell growth; B. Clone formation assays demonstrated a significant decrease in cell clone formation efficiency in the shPRKD3 groups compared to the shNC group in Huh7 cells; C. Cell proliferation was decreased after PRKD3 knockdown detected by 5-Ethynyl-2'-deoxyuridine (EdU) staining. Results are displayed as the mean ± SD. **$P < 0.01$, n=3.

Identification of differentially expressed proteins

To explore the regulatory role of PRKD3 in the malignant biological process of liver cancer, proteomic analysis was conducted on five samples from both the shNC and shPRKD3 groups. A total of 330 proteins exhibited differential expression between the control shNC group and shPRKD3 group, with 153 proteins upregulated and 177 downregulated. The volcano plot depicted the quantification results, highlighting the top 10 differentially expressed proteins, including HMGCS2, SPART, GC, TLN2, ACSM2B for upregulation, and FTH1, SERPINE1, GDF15, MYOF, WWC1 for downregulation (**Figure 5A**). Cluster analysis of DEPs revealed distinct expression patterns between the two cell groups, with shNC cells clustering together, and PRKD3 knockdown cells forming a separate cluster (**Figure 5B**).

GO enrichment analysis

Based on the GO database, upregulated and downregulated proteins were enriched in the top 5 GO ontology terms for BP, CC, and MF. These terms include isoleucine transport, cellular response to mechanical stimulus, positive regulation of apoptotic process, fatty acid biosynthetic process for BP; extracellular exosome, collagen-containing extracellular matrix, mitochondrion for CC; and integrin binding, proteoglycan binding for MF (**Figure 6A-C**).
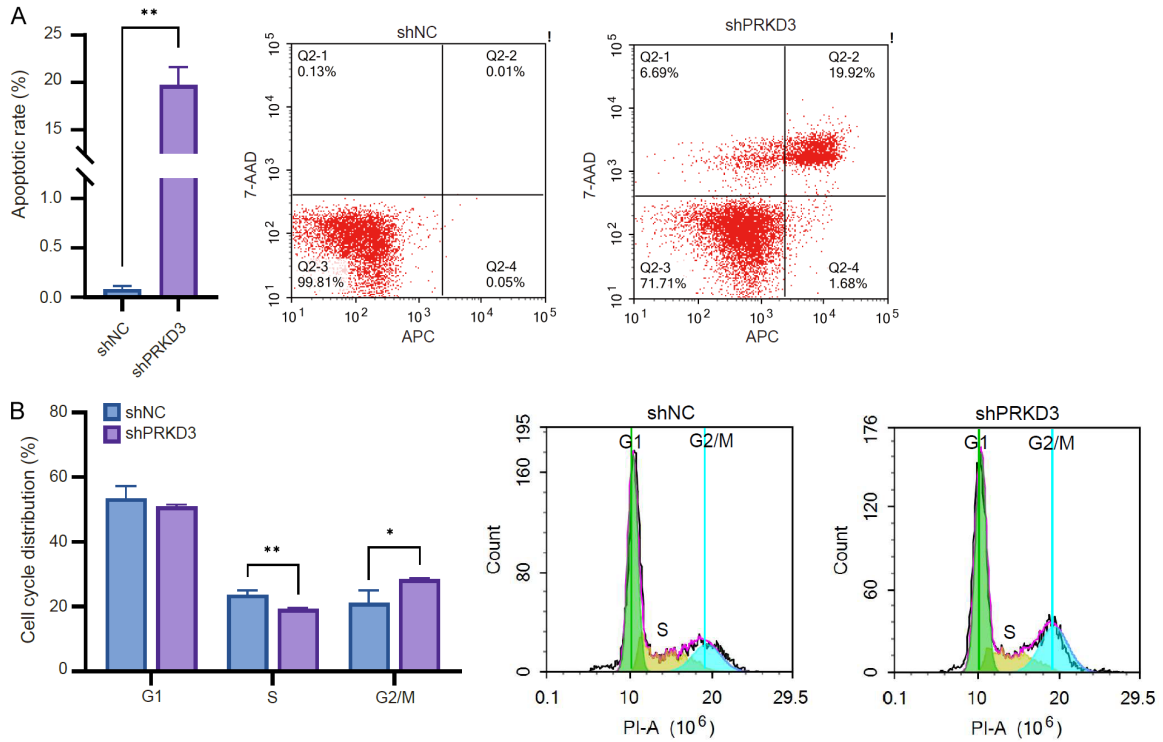
Figure 4. Knockdown of PRKD3 induced apoptosis and cell cycle arrest. A. Analysis of apoptosis of Huh7 cells before and after PRKD3 knockdown; B. Analysis of cell cycles by flow cytometry. The bar graph also displays cell distribution across cell cycle phases. Results are displayed as the mean ± SD. *$P < 0.05$; **$P < 0.01$, n=3.
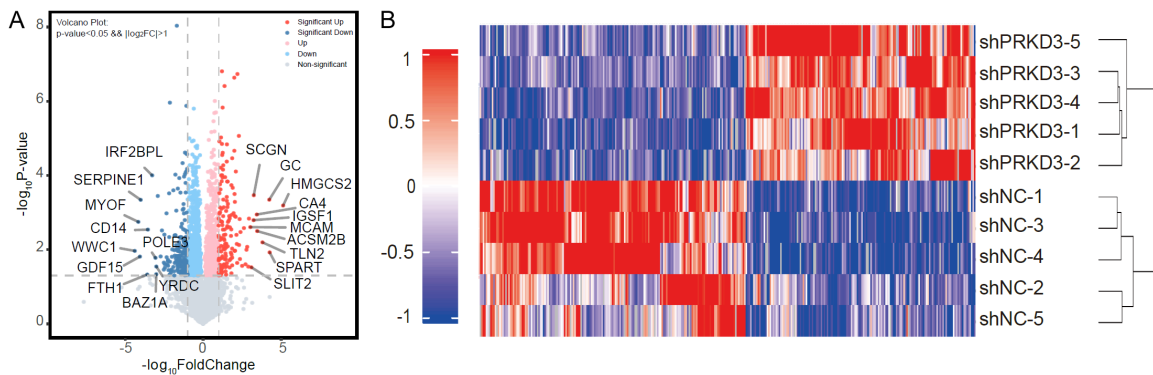

Figure 5. Volcano map and hierarchical clustering results of differentially expressed proteins. A. In the volcano map, each point signifies a gene, with the horizontal and vertical axes indicating the logarithmic values of the fold change (FC) between the shPRKD3 group and the shNC group. This visualization facilitated the identification of genes with significant differential expression. B. The hierarchical clustering results depict each gene as a small square, where the color represents the expression level of that gene. A tree diagram to the right illustrated the clustering analysis results of different samples from various experimental groups.

KEGG enrichment analysis

DEPs were further analyzed for enrichment in KEGG pathways, highlighting their association with cancer metabolism, immunity, proliferation, and metastasis. Key pathways identified include ferroptosis, complement and coagulation cascades, lysosome, AMPK signaling pathway, ECM-receptor interaction, autophagy, and tight junctions. The top 20 enriched KEGG pathways are depicted in **Figure 7B**, showing the significant involvement of proteins such as CDK4 and SERPINE1 across multiple tumor-related pathways (**Figure 7A-C**).
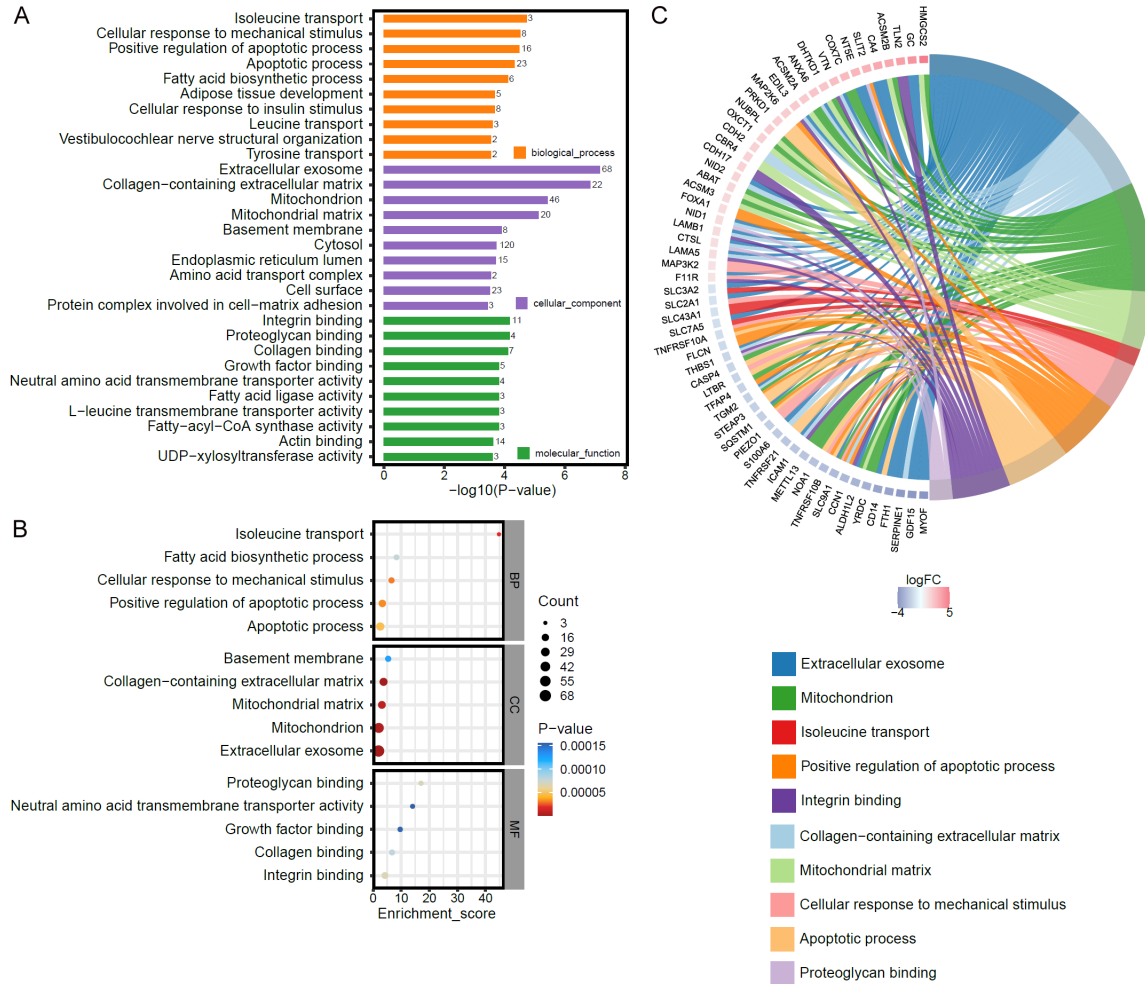
Figure 6. Gene Ontology (GO) enrichment analysis results. A. The chart shows the top 5 GO terms with the highest number of differentially expressed protein annotations across different categories. The horizontal axis displays the $-log_{10}p$, while the vertical axis lists the names of the GO terms, with the number on each column indicating the count of proteins annotated to that term. B. This part highlights the top 5 GO terms with the highest enrichment levels across different categories. The Enrichment Score is shown on the horizontal axis, with the top 5 terms for biological process (BP), cellular compartment (CC), and molecular function (MF) on the vertical axis. Bubble size and color vary to represent the quantity of proteins contained within each term and the significance of enrichment, respectively; redder hues indicate smaller p values and higher significance. C. This part displays GO terms enriched among major differential protein annotations, focusing on the 10 entries with List Hits greater than 2 and the smallest p for a GO chord diagram. This illustrates the relationship between selected GO terms and their corresponding key proteins: protein gene names with upregulation are shown in red while downregulation is indicated in blue on the left side, and the selected GO terms are listed on the right side.

PPI network analysis

By constructing a PPI network, extensive interactions between differential proteins were identified. Proteins such as CDH1, CDK4, CDK2, SERPINE1, SMAD3, and SQSTM1 were found to occupy core positions within the network (Supplementary Figure 1). Additionally, the top 25 core proteins with the highest connectivity were selected for further verification, constructing an interaction network diagram. This sug-

gests that these core proteins might be potential downstream key proteins by which PRKD3 regulates the function of liver cancer cells (**Figure 8**).

The selected proteins were validated through Western blot analysis

To confirm the proteomics data, five differentially expressed proteins (CDK4, SERPINE1, and SQSTM1) with key functions were detected
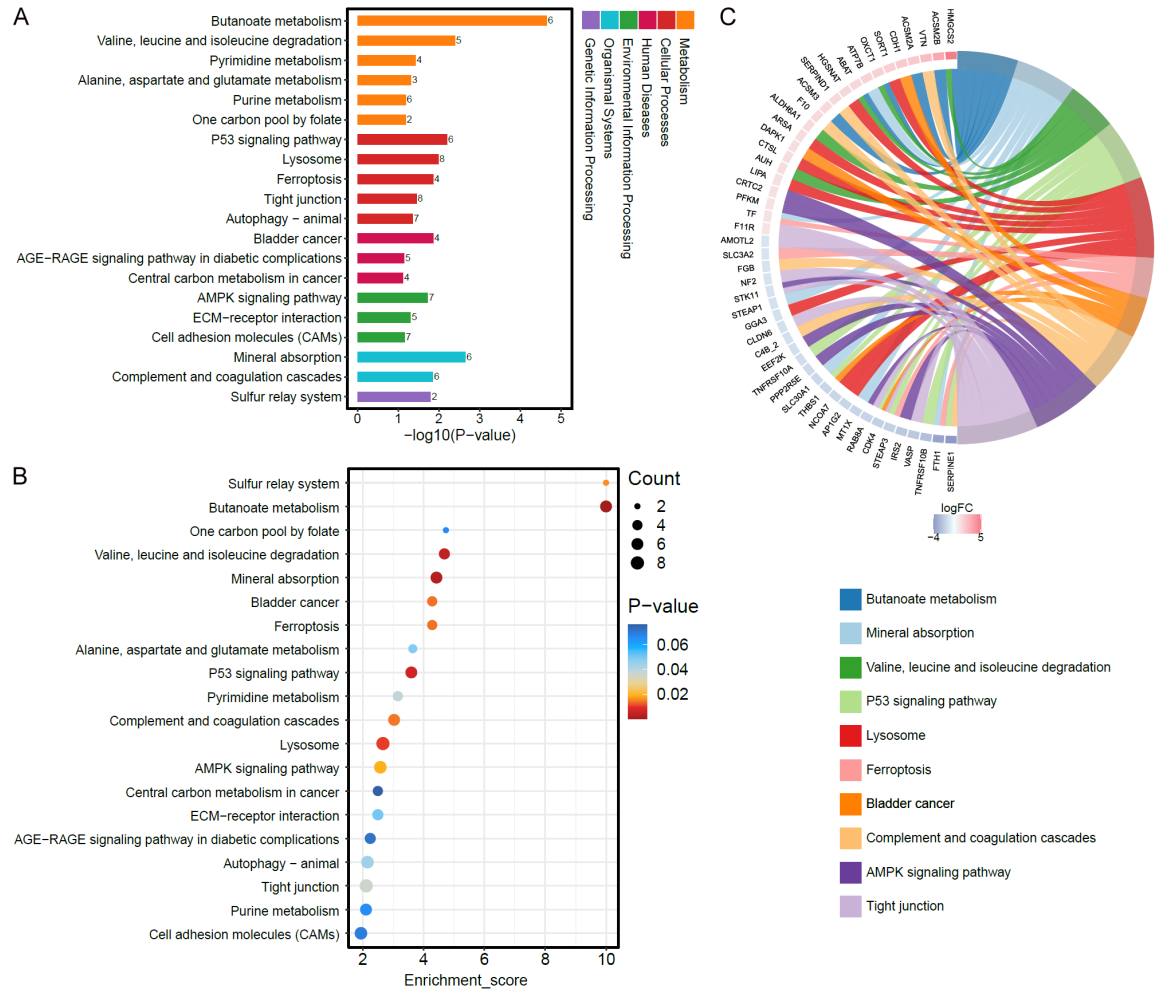
Figure 7. Kyoto Encyclopedia of Genes and Genomes (KEGG) enrichment analysis results. A. Distribution map of differential proteins at KEGG Level 1 (the 20 pathways with the smallest *p* value): The horizontal axis displays the -log$_{10}$p for each pathway, the vertical axis lists different pathway names, and the number on each column indicates the count of proteins annotated to that pathway. Different column colors represent different KEGG Level 1 categories. B. Top 20 KEGG enrichment analysis bubble chart: The horizontal axis represents the enrichment score, and the vertical axis lists the top 20 pathways. Larger bubbles indicate a greater number of proteins, with bubble color changing from blue to red indicating a smaller and more significant enriched *p* value. C. KEGG enrichment analysis chord diagram: This represents the 10 pathways with List Hits greater than 3 and the smallest *p* value, illustrating the relationship between selected pathways and their corresponding key proteins. The left side shows protein gene names, with red for upregulation and blue for downregulation, while the right side displays the selected KEGG pathways.

using Western blot analysis. At the same time, due to the significant changes in the autophagy pathway, an enriched signaling pathway in KEGG, we also selected other differentially expressed proteins, RAB8A and NRBF2, in the autophagy signaling pathway for validation detection of expression levels. Consistent with the proteome analysis results, the validation showed that the expression levels of all five proteins were significantly downregulated (**Figure 9**).

Discussion

The analysis of the TCGA clinical dataset revealed that PRKD3 was highly expressed in liver cancer and significantly associated with poor prognosis in liver cancer patients, indicating its role as an oncoprotein in liver cancer cells. Further *in vitro* experiments demonstrated that knocking down PRKD3 could significantly inhibit the proliferation of Huh7 cells, increase apoptosis, and cause cell cycle arrest
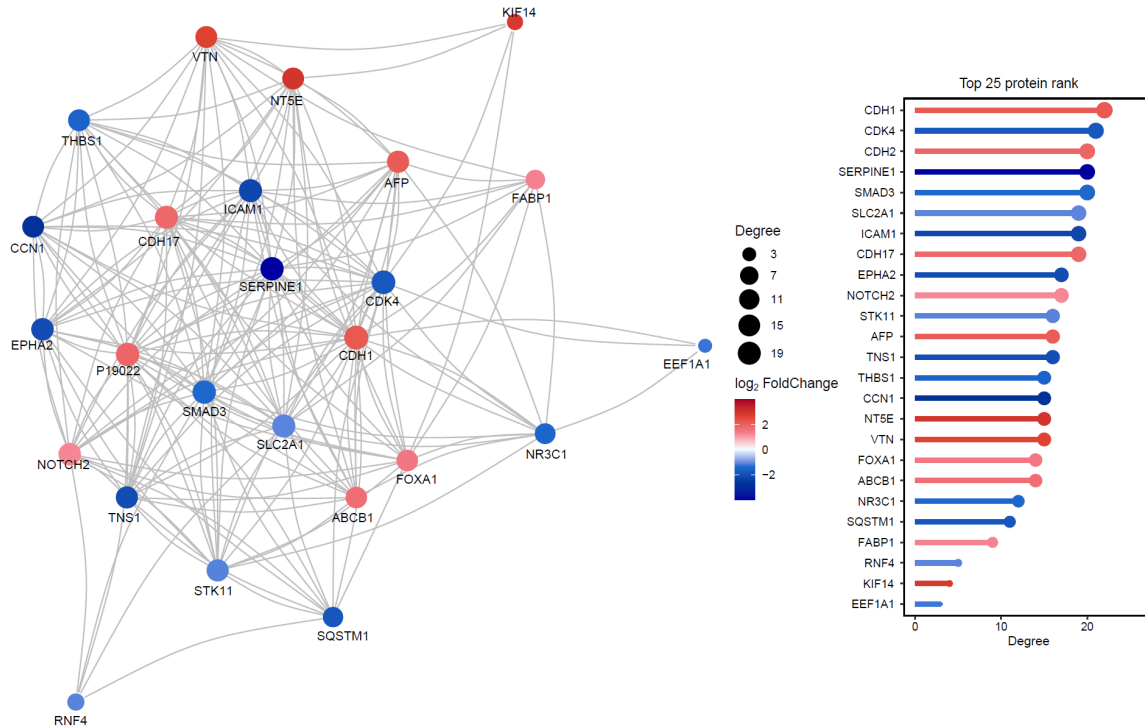
Figure 8. Top 25 connectivity protein interaction network diagram. This diagram represents differentially expressed proteins, with upregulation shown in red and downregulation in blue. The size of each circle indicates the level of connectivity, with larger circles denoting higher connectivity. A bar chart on the right displays the expression of the top 25 connectivity proteins.
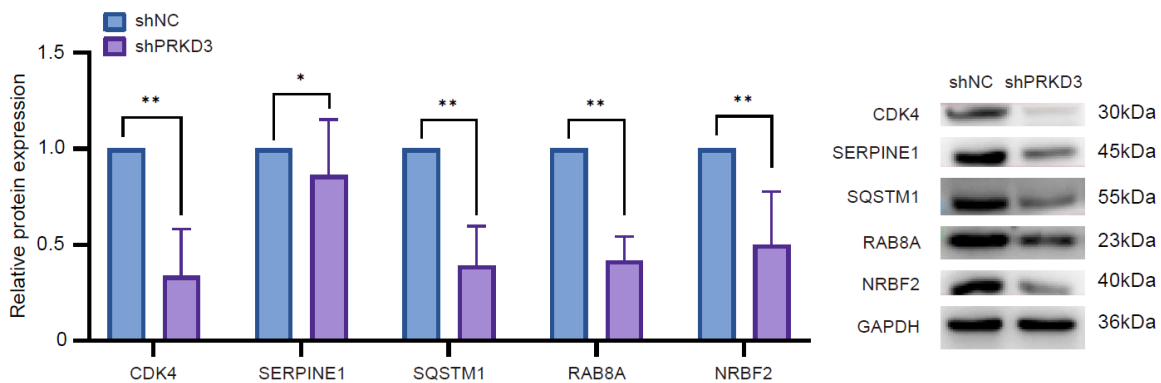

Figure 9. Detection of key proteins and pathway related proteins. Results are displayed as the mean ± SD. *P < 0.05; **P < 0.01, n=3.

in the G2/M phase. Bioinformatic analysis showed the differentially expressed proteins resulting from PRKD3 knockdown were enriched in processes such as cell apoptosis and autophagy, as well as signaling pathways closely related with tumor growth and cell death, including the p53 and AMPK signaling pathways. The regulation of cell proliferation is one

of the earliest reported biological functions of PRKD [12, 13]. Kienzle et al. declared that PRKD knockout could lead to cell cycle arrest in the G2 phase and fragmentation of the Golgi apparatus via the Raf-MEK1 signaling pathway, preventing cells from entering mitosis by cell cycle arrest [14]. Our findings align with this, suggesting that the regulation of cell cycle-

related proteins may be an important mechanism by which PRKD influences cancer cell proliferation.

CDK4, a cyclin regulatory protein and serine/threonine kinase, regulates cell cycle transition by phosphorylating and inhibiting members of the retinoblastoma (RB) protein family. The CDK4 complex serves as a key mediator, integrating diverse mitotic and anti-mitotic signals. It phosphorylates SMAD3 in a cell cycle-dependent manner and inhibits its transcriptional activity [15-17]. In our proteomics analysis, SMAD3 was identified as one of the differentially expressed proteins. Previous studies have highlighted CDK4's interactions with p53 family members and its anti-apoptotic effects [18-20]. Our study further indicates that PRKD3 knockdown reduces the expression of CDK4, suggesting that CDK4 might be a crucial downstream protein through which PRKD3 exerts its oncogenic role in liver cancer.

SERPINE1, also known as plasminogen activator inhibitor-1 (PAI-1), is a member of the serine protease inhibitor (SERPIN) family and serves as a major inhibitor of the plasminogen activation system. Changes in SERPINE1 expression have been observed in various cancers [21, 22], highlighting its role as an oncoprotein and a potential therapeutic target. It could promote tumor cell growth through its proangiogenic activity and anti-apoptotic properties [23-27]. Downregulation of SERPINE1 expression could halt the cell cycle transitioning from G0 to G1 phase, thereby inhibiting cell proliferation. Conversely, overexpression of SERPINE1 promotes proliferation by facilitating cell entry into the S phase. The cell cycle regulatory function of SERPINE1 is linked to the depletion of cyclin D3/CDK4/6 [28].

SQSTM1, known as P62, serves as a key protein in the ubiquitination system and functions as a receptor in selective autophagy, crucial for regulating intracellular protein degradation and maintaining cellular homeostasis. Bioinformatic analyses and clinical studies have shown that SQSTM1 is overexpressed in various tumor cells, promoting cancer cell development [29]. Ashley Sample et al. demonstrated that SQSTM1 is essential for skin tumor growth *in vivo*, emphasizing its role as an oncogene [30]. Notably, SQSTM1 overexpression alone, even in the absence of carcinogens or other irritants, is sufficient to induce HCC [31]. Additionally, SQSTM1 can continuously activate NRF2, impacting glucose and glutamine metabolism and significantly promoting cancer cell survival [32]. Previous research has indicated that abnormal glucose metabolism is a poor prognostic factor in liver cancer. Regarding signaling pathway regulation, SQSTM1 influences tumor cell proliferation by regulating the AKT/AMPK/mTOR signaling pathway and initiating autophagy [29]. These pathways are intricately linked to cancer cell metabolism. The expression changes in SQSTM1 along with the functional enrichment in apoptosis and autophagy regulation upon PRKD3 knockdown suggest that SQSTM1 could act as a critical downstream protein in the mechanism by which PRKD3 regulated tumor functionality.

RAB8A and NRBF2 proteins, exhibiting differential expression, play crucial roles in autophagy function enrichment. RAB8A, a member of the small GTPases family, is instrumental in regulating intracellular membrane trafficking, overseeing processes from transport vesicle formation to membrane fusion [33]. The active form of RAB8A could recruit TBK1, initiating the autophagic clearance of target proteins by activating SQSTM1 phosphorylation. Concurrently, reduced RAB8A expression could reduce cell growth by inhibiting the AKT and ERK1/2 signaling pathways and promote cell apoptosis by modulating the expression of apoptotic markers such as Caspase3-P17, Bax, and Bcl-2 [34, 35].

Nuclear receptor binding factor 2 (NRBF2), a transcriptional activator, is associated with poor tumor prognosis. It directly interacts with p62 to regulate autophagy function [36]. Additionally, NRBF2 could regulate the chemoresistance of small cell lung cancer by interacting with the P62 protein in the autophagy process and is vital for the clearance of apoptotic cells. The lack of NRBF2 expression blocks the transition from RAB5A-positive early phagosomes to RAB7-positive late phagosomes, resulting in the accumulation of apoptotic cells [37].

Our study indicates the influence of PRKD3 on growth, apoptosis, and the cell cycle in liver cancer. We also identified potential signaling pathways and differentially expressed proteins related with PRKD3. Further research will focus

on exploring the functions with these validated DEPs and signaling pathways they are involved in.

Conclusions

In conclusion, the findings highlight the inhibitory effect of PRKD3 knockdown on HCC proliferation and unveils the proteomic features of PRKD3 regulation. CDK4, SERPINE1, SQSTM1, RAB8A, and NRBF2 may serve as key proteins in regulatory functions.

Acknowledgements

Disclosure of conflict of interest

None.

Address correspondence to: Linjing Li, Department of Clinical Laboratory Center, Lanzhou University Second Hospital, No. 82 Cuiyingmen, Chengguan District, Lanzhou 730030, Gansu, China. Tel: +86-13519650086; E-mail: lilinj@lzu.edu.cn

References

[1] Huck B, Duss S, Hausser A and Olayioye MA. Elevated protein kinase D3 (PKD3) expression supports proliferation of triple-negative breast cancer cells and contributes to mTORC1-S6K1 pathway activation. J Biol Chem 2014; 289: 3138-3147.

[2] Liu Y, Li J, Ma Z, Zhang J, Wang Y, Yu Z, Lin X, Xu Z, Su Q, An L, Zhou Y, Ma X, Yang Y, Wang F, Chen Q, Zhang Y, Wang J, Zheng H, Shi A, Yu S, Zhang J, Zhao W and Chen L. Oncogenic functions of protein kinase D2 and D3 in regulating multiple cancer-related pathways in breast cancer. Cancer Med 2019; 8: 729-741.

[3] Lieb WS, Lungu C, Tamas R, Berreth H, Rathert P, Storz P, Olayioye MA and Hausser A. The GEF-H1/PKD3 signaling pathway promotes the maintenance of triple-negative breast cancer stem cells. Int J Cancer 2020; 146: 3423-3434.

[4] Döppler H, Bastea LI, Borges S, Spratley SJ, Pearce SE and Storz P. Protein kinase d isoforms differentially modulate cofilin-driven directed cell migration. PLoS One 2014; 9: e98090.

[5] Chen J, Deng F, Singh SV and Wang QJ. Protein kinase D3 (PKD3) contributes to prostate cancer cell growth and survival through a PKCepsilon/PKD3 pathway downstream of Akt and ERK 1/2. Cancer Res 2008; 68: 3844-3853.

[6] Li L, Hua L, Fan H, He Y, Xu W, Zhang L, Yang J, Deng F and Zeng F. Interplay of PKD3 with SREBP1 promotes cell growth via upregulating lipogenesis in prostate cancer cells. J Cancer 2019; 10: 6395-6404.

[7] LaValle CR, Zhang L, Xu S, Eiseman JL and Wang QJ. Inducible silencing of protein kinase D3 inhibits secretion of tumor-promoting factors in prostate cancer. Mol Cancer Ther 2012; 11: 1389-1399.

[8] Zhang J, Zhang Y, Wang J, Zhang S, Zhao Y, Ren H, Chu Y, Feng L and Wang C. Protein kinase D3 promotes gastric cancer development through p65/6-phosphofructo-2-kinase/fructose-2,6-biphosphatase 3 activation of glycolysis. Exp Cell Res 2019; 380: 188-197.

[9] He JH, Li BX, Han ZP, Zou MX, Wang L, Lv YB, Zhou JB, Cao MR, Li YG and Zhang JZ. Snail-activated long non-coding RNA PCA3 up-regulates PRKD3 expression by miR-1261 sponging, thereby promotes invasion and migration of prostate cancer cells. Tumour Biol 2016; [Epub ahead of print].

[10] Zou Z, Zeng F, Xu W, Wang C, Ke Z, Wang QJ and Deng F. PKD2 and PKD3 promote prostate cancer cell invasion by modulating NF-κB- and HDAC1-mediated expression and activation of uPA. J Cell Sci 2012; 125: 4800-4811.

[11] Yang H, Xu M, Chi X, Yan Q, Wang Y, Xu W, Zhuang K, Li A and Liu S. Higher PKD3 expression in hepatocellular carcinoma (HCC) tissues predicts poorer prognosis for HCC patients. Clin Res Hepatol Gastroenterol 2017; 41: 554-563.

[12] Zhukova E, Sinnett-Smith J and Rozengurt E. Protein kinase D potentiates DNA synthesis and cell proliferation induced by bombesin, vasopressin, or phorbol esters in Swiss 3T3 cells. J Biol Chem 2001; 276: 40298-40305.

[13] Rennecke J, Rehberger PA, Fürstenberger G, Johannes FJ, Stöhr M, Marks F and Richter KH. Protein-kinase-Cmu expression correlates with enhanced keratinocyte proliferation in normal

and neoplastic mouse epidermis and in cell culture. Int J Cancer 1999; 80: 98-103.

[14] Kienzle C, Eisler SA, Villeneuve J, Brummer T, Olayioye MA and Hausser A. PKD controls mitotic Golgi complex fragmentation through a Raf-MEK1 pathway. Mol Biol Cell 2013; 24: 222-233.

[15] Matsuura I, Denissova NG, Wang G, He D, Long J and Liu F. Cyclin-dependent kinases regulate the antiproliferative function of Smads. Nature 2004; 430: 226-231.

[16] Wang Z, Xie Y, Zhang L, Zhang H, An X, Wang T and Meng A. Migratory localization of cyclin D2-Cdk4 complex suggests a spatial regulation of the G1-S transition. Cell Struct Funct 2008; 33: 171-183.

[17] Kitagawa M, Higashi H, Jung HK, Suzuki-Takahashi I, Ikeda M, Tamai K, Kato J, Segawa K, Yoshida E, Nishimura S and Taya Y. The consensus motif for phosphorylation by cyclin D1-Cdk4 is different from that for phosphorylation by cyclin A/E-Cdk2. EMBO J 1996; 15: 7060-7069.

[18] Sheppard KE and McArthur GA. The cell-cycle regulator CDK4: an emerging therapeutic target in melanoma. Clin Cancer Res 2013; 19: 5320-5328.

[19] Aggarwal P, Vaites LP, Kim JK, Mellert H, Gurung B, Nakagawa H, Herlyn M, Hua X, Rustgi AK, McMahon SB and Diehl JA. Nuclear cyclin D1/CDK4 kinase regulates CUL4 expression and triggers neoplastic growth via activation of the PRMT5 methyltransferase. Cancer Cell 2010; 18: 329-340.

[20] Li Y, Chitnis N, Nakagawa H, Kita Y, Natsugoe S, Yang Y, Li Z, Wasik M, Klein-Szanto AJ, Rustgi AK and Diehl JA. PRMT5 is required for lymphomagenesis triggered by multiple oncogenic drivers. Cancer Discov 2015; 5: 288-303.

[21] Van De Craen B, Declerck PJ and Gils A. The biochemistry, physiology and pathological roles of PAI-1 and the requirements for PAI-1 inhibition in vivo. Thromb Res 2012; 130: 576-585.

[22] Vaughan DE, Rai R, Khan SS, Eren M and Ghosh AK. Plasminogen activator inhibitor-1 is a marker and a mediator of senescence. Arterioscler Thromb Vasc Biol 2017; 37: 1446-1452.

[23] Li Y, Yu H, Han X and Pan Y. Analyses of hypoxia-related risk factors and clinical relevance in breast cancer. Front Oncol 2024; 14: 1350426.

[24] Huang X, Wang L, Guo H and Zhang W. Single-cell RNA sequencing reveals SERPINE1-expressing CAFs remodelling tumour microenvironment in recurrent osteosarcoma. Clin Transl Med 2024; 14: e1527.

[25] Bajou K, Peng H, Laug WE, Maillard C, Noel A, Foidart JM, Martial JA and DeClerck YA. Plasminogen activator inhibitor-1 protects endothelial cells from FasL-mediated apoptosis. Cancer Cell 2008; 14: 324-334.

[26] Madunić J. The urokinase plasminogen activator system in human cancers: an overview of its prognostic and predictive role. Thromb Haemost 2018; 118: 2020-2036.

[27] Zhang W, Zhang M, Sun M, Hu M, Yu M, Sun J, Zhang X and Du B. Metabolomics-transcriptomics joint analysis: unveiling the dysregulated cell death network and developing a diagnostic model for high-grade neuroblastoma. Front Immunol 2024; 14: 1345734.

[28] Giacoia EG, Miyake M, Lawton A, Goodison S and Rosser CJ. PAI-1 leads to G1-phase cell-cycle progression through cyclin D3/cdk4/6 upregulation. Mol Cancer Res 2014; 12: 322-334.

[29] Yu F, Ma R, Liu C, Zhang L, Feng K, Wang M and Yin D. SQSTM1/p62 promotes cell growth and triggers autophagy in papillary thyroid cancer by regulating the AKT/AMPK/mTOR signaling pathway. Front Oncol 2021; 11: 638701.

[30] Sample A, Zhao B, Qiang L and He YY. Adaptor protein p62 promotes skin tumor growth and metastasis and is induced by UVA radiation. J Biol Chem 2017; 292: 14786-14795.

[31] Umemura A, He F, Taniguchi K, Nakagawa H, Yamachika S, Font-Burgada J, Zhong Z, Subramaniam S, Raghunandan S, Duran A, Linares JF, Reina-Campos M, Umemura S, Valasek MA, Seki E, Yamaguchi K, Koike K, Itoh Y, Diaz-Meco MT, Moscat J and Karin M. p62, Upregulated during preneoplasia, induces hepatocellular carcinogenesis by maintaining survival of stressed HCC-initiating cells. Cancer Cell 2016; 29: 935-948.

[32] Saito T, Ichimura Y, Taguchi K, Suzuki T, Mizushima T, Takagi K, Hirose Y, Nagahashi M, Iso T, Fukutomi T, Ohishi M, Endo K, Uemura T, Nishito Y, Okuda S, Obata M, Kouno T, Imamura R, Tada Y, Obata R, Yasuda D, Takahashi K, Fujimura T, Pi J, Lee MS, Ueno T, Ohe T, Mashino T, Wakai T, Kojima H, Okabe T, Nagano T, Motohashi H, Waguri S, Soga T, Yamamoto M, Tanaka K and Komatsu M. p62/Sqstm1 promotes malignancy of HCV-positive hepatocellular carcinoma through Nrf2-dependent metabolic reprogramming. Nat Commun 2016; 7: 12030.

[33] Aizawa M and Fukuda M. Small GTPase Rab2B and its specific binding protein golgi-associated Rab2B interactor-like 4 (GARI-L4) regulate golgi morphology. J Biol Chem 2015; 290: 22250-22261.

[34] Heo JM, Ordureau A, Paulo JA, Rinehart J and Harper JW. The PINK1-PARKIN mitochondrial

ubiquitylation pathway drives a program of OPTN/NDP52 recruitment and TBK1 activation to promote mitophagy. Mol Cell 2015; 60: 7-20.

[35] Freischmidt A, Wieland T, Richter B, Ruf W, Schaeffer V, Müller K, Marroquin N, Nordin F, Hübers A, Weydt P, Pinto S, Press R, Millecamps S, Molko N, Bernard E, Desnuelle C, Soriani MH, Dorst J, Graf E, Nordström U, Feiler MS, Putz S, Boeckers TM, Meyer T, Winkler AS, Winkelman J, de Carvalho M, Thal DR, Otto M, Brännström T, Volk AE, Kursula P, Danzer KM, Lichtner P, Dikic I, Meitinger T, Ludolph AC, Strom TM, Andersen PM and Weishaupt JH. Haploinsufficiency of TBK1 causes familial ALS and fronto-temporal dementia. Nat Neurosci 2015; 18: 631-636.

[36] Shen W, Luo P, Sun Y, Zhang W, Zhou N, Zhan H, Zhang Q, Shen J, Lin A, Cheng Q, Wang Q, Zhang J, Wang HH and Wei T. NRBF2 regulates the chemoresistance of small cell lung cancer by interacting with the P62 protein in the autophagy process. iScience 2022; 25: 104471.

[37] Wu MY, Liu L, Wang EJ, Xiao HT, Cai CZ, Wang J, Su H, Wang Y, Tan J, Zhang Z, Wang J, Yao M, Ouyang DF, Yue Z, Li M, Chen Y, Bian ZX and Lu JH. PI3KC3 complex subunit NRBF2 is required for apoptotic cell clearance to restrict intestinal inflammation. Autophagy 2021; 17: 1096-1111.

PRKD3 in HCC cells
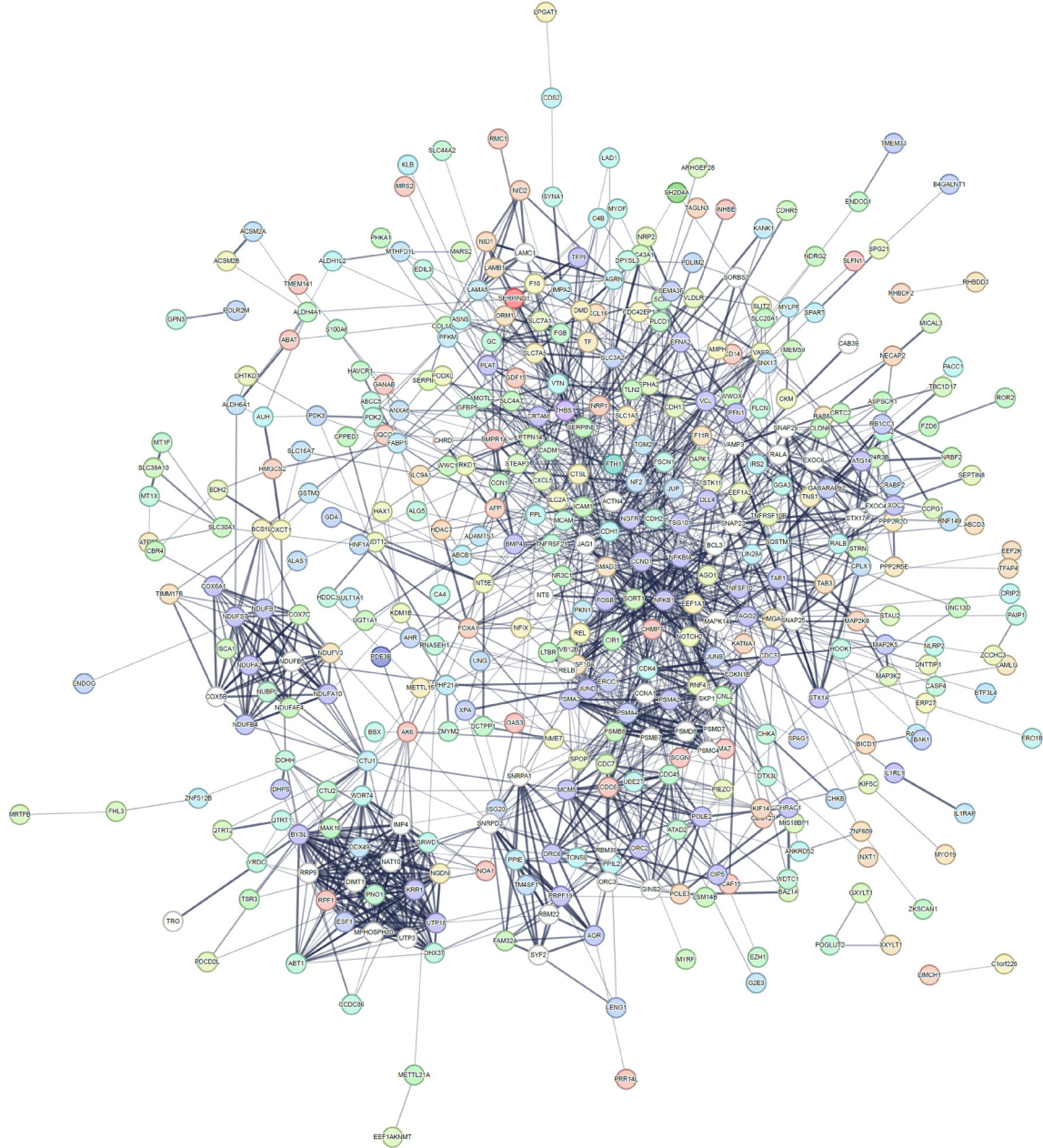
Supplementary Figure 1. Differentially expressed protein interaction network.